The following publication A. Haddadi, M. Zhao, I. Kocar, U. Karaagac, K. W. Chan and E. Farantatos, "Impact of Inverter-Based Resources on Negative Sequence Quantities-Based Protection Elements," in IEEE Transactions on Power Delivery, vol. 36, no. 1, pp. 289-298, Feb. 2021 is available at https://doi.org/10.1109/TPWRD.2020.2978075

Impact of Inverter-Based Resources on Negative Sequence Quantities-Based Protection Elements

Aboutaleb Haddadi, *Member, IEEE,* Mingxuan Zhao, *Student Member, IEEE,* Ilhan Kocar, *Senior Member, IEEE,* Ulas Karaagac, *Member, IEEE,* Ka Wing Chan, *Member, IEEE*, and Evangelos Farantatos, *Senior Member, IEEE*

***Abstract*—Inverter-Based Resources (IBRs), including Wind turbine generators (WTGs), exhibit substantially different negative-sequence fault current characteristics compared to synchronous generators (SGs). These differences may cause misoperation of customary negative-sequence-based protective elements set under the assumption of a conventional SG dominated power system. The amplitude of the negative-sequence fault current of a WTG is smaller than that of an SG. This may lead to misoperation of the negative-sequence overcurrent elements 50Q/51Q. Moreover, the angular relation of the negative-sequence current and voltage is different under WTGs, which may result in the misoperation of directional negative-sequence overcurrent element 67Q. This paper first studies the key differences between the WTGs and SG by comparing their equivalent negative-sequence impedances with SG's. Then, simulation case studies are presented showing the misoperation of 50Q and 67Q due to wind generation and the corresponding impact on communication-assisted protection and fault identification scheme (FID). The impact on directional element is also experimentally validated in a hardware-in-the-loop real-time simulation set up using a physical relay. Finally, the paper studies the impact of various factors such as WTG type (Type-III/Type-IV) and Type-IV WTG control scheme (coupled/decoupled sequence) to determine the key features that need to be considered in practical protection studies. The objective is to show potential protection misoperation issues, identify the cause, and propose potential solutions.**

***Index Terms*—Power system protection, Negative sequence component, Negative-sequence overcurrent protection, Directional negative-sequence overcurrent, Inverter-based resource, Wind farms, Full-size converter, Doubly-fed induction generator, Power system modeling.**

I. Introduction

THE increase in the integration of wind parks (WPs) and other inverter-based resources (IBRs) presents technical challenges for system protection [1],[2]. WPs consist of wind turbine generators (WTGs) that have fault response characteristics different from traditional synchronous rotating generators. The converter control scheme [3]–[13] has a major role in the response of WTGs. Therefore, there is a surge of interest on their impact on system protection [1], [2] and the performance of various legacy protection schemes including distance [14]–[18] and power swing protection [19] schemes. The focus of this paper is the negative sequence quantities-based schemes.

WTGs exhibit different negative-sequence fault current characteristics compared to synchronous generators (SGs). The negative-sequence fault current contribution of the WTG can be very small depending on its type and control [20]–[23] as there is no specific requirement in most grid codes. This small negative-sequence fault current contribution may result in the misoperation of protection elements such as negative-sequence overcurrent (50Q and 51Q) whose operation relies on the assumption of significant negative sequence currents during unbalanced faults. The recent German grid code VDE-AR-N 4120 [24] imposes a proportional reactive negative sequence current component as a function of the variation of negative sequence voltage. This may provide enough negative sequence current with desired angular relation of negative-sequence voltages and currents. If WTG controllers do not impose the angular relation, this may result in the misoperation of directional negative-sequence overcurrent (67Q) element, which uses angular relation to detect fault direction [21]. Considering that 50Q, 51Q, and 67Q are used in a number of protection functions such as communication-assisted protection and fault identification scheme (FID), their misoperation poses a reliability problem.

The objective of this paper is to study the impact of wind generation on the performance of negative sequence quantities-based protection elements, identify potential protection misoperation issues and evaluate possible solutions. The paper considers Type-III WTG with traditional coupled sequence control (CSC), Type-IV WTG with traditional CSC and Type-IV WTG with decoupled sequence control (DCS) compliant with VDE-AR-N 4120. Reference [25] has presented the implementation of the DSC used in this paper. While the paper

A. Haddadi, M. Zhao, and I. Kocar are with Polytechnique Montreal, Montreal, QC H3T1J4 Canada (e-mail: aboutaleb.haddadi@polymtl.ca, mingxuan.zhao@polymtl.ca, ilhan.kocar@polymtl.ca).

U. Karaagac and K.W. Chan are with the Hong Kong Polytechnic University, Hung Hom, Hong Kong (e-mail: ulas.karaagac@polymtl.ca eekwchan@polyu.edu.hk).

E. Farantatos is with the Electric Power Research Institute (EPRI), Palo Alto, CA, U.S. (e-mail: efarantatos@epri.com).

does not explicitly consider photovoltaic (PV)-based resources, the findings of Type-IV WTG in principle and mostly apply to transmission-level PV-based resources. First, the equivalent negative-sequence impedances of WTGs are compared with SG's to explain the key differences between the negative-sequence fault current characteristics of WTGs and SG. It should be emphasized that, the negative sequence fault current contribution of Type-III WTG is compliant with VDE-AR-N 4120 while operating under traditional CSC. Then, the paper demonstrates the impact of these differences on protection system on a multi WP practical system through electromagnetic transient (EMT) simulations. The illustrated misoperation examples include 50Q and 67Q elements as well as communication-assisted protection and FID. The last part presents the real-time (RT) hardware-in-the-loop (HIL) validation of one of the EMT simulations using an actual relay. WP operating conditions such as the number of WTG units in service and wind speed are other influential factors but left out in this paper due to page limits.

II. Negative-sequence Impedance of a Wind Turbine Generator vs. Synchronous Generator

To illustrate the difference in negative-sequence fault current characteristics of IBRs and SGs, this section uses an equivalent impedance representation of these generators under short-circuit conditions. The impedance representation is developed assuming steady-state conditions based on a nominal-frequency phasor model.

Under unbalanced network conditions or faults, a voltage containing a negative-sequence component is imposed at the terminal of a WTG, as shown in Fig. 1, causing the WTG to inject a negative-sequence current, which can be written as

$$\bar{I}_{WTG} = -\left(\frac{1}{\bar{Z}_{WTG}}\right)\bar{V}_{WTG}, \quad \text{with} \quad \bar{Z}_{WTG} = \left|\bar{Z}_{WTG}\right| \angle \bar{\varphi}_{Z_{WTG}}, \qquad (1)$$

where $\bar{V}_{WTG}$ denotes the phasor of the negative-sequence voltage at the point of grid coupling (PGC), $\bar{I}_{WTG}$ represents the phasor of the negative-sequence current of the WTG flowing into the grid, $\bar{Z}_{WTG}$ signifies the equivalent negative-sequence impedance of the WTG seen from the PGC, and $\left|\bar{Z}_{WTG}\right|$ and $\bar{\varphi}_{Z_{WTG}}$ represent the amplitude and phase angle of this impedance, respectively.

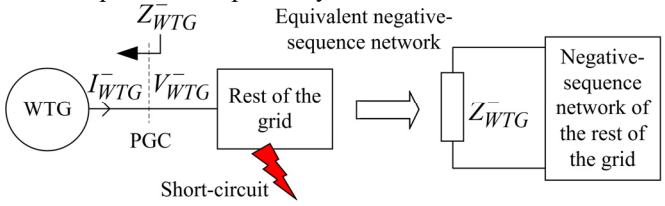

Fig. 1. Representation of a WTG by an equivalent impedance in the negative sequence network for short circuit analysis.

The equivalent negative-sequence impedance of a WTG depends on the type. Type-IV uses a full-size converter (FSC), and hence, the negative-sequence impedance characteristics depend on the converter control scheme. Type-III uses a doubly-fed induction generator (DFIG), and hence, the negative-sequence impedance depends on both the control system and the machine.

A. FSC WTG with CSC

Readers should refer to [25] for more details on the FSC WP model used in this paper. The WP is an aggregated model of 1.5-MW permanent magnet synchronous generator (PMSG)-based WTGs interfaced to the grid through a collector grid and a wind park transformer. The fault behavior of this EMT model has been validated for traditional CSC using fault records of a PV solar plant in [23] by replacing the wind turbine side of the DC bus with PV arrays.

The calculation of the equivalent negative-sequence impedance breaks down to finding a relation between $\bar{I}_{WTG}$ and $\bar{V}_{WTG}$ through the control loop. Reference [26] has shown that the negative-sequence impedance of an FSC WTG can be written as

$$\bar{Z}_{WTG} = \frac{R + jX + H_{filter}\left(H_{PI}^{g} - R + jX\right)}{\left(1 - H_{filter}\right)}, \qquad (2)$$

where R is the resistance of the choke filter and X is the reactance of the choke filter at nominal frequency. H_{PI}^{g} is the complex gain of the inner PI current controller at twice the nominal frequency given by $H_{PI}^{g} = K_P + \frac{K_I}{j4\pi f_{nom}}$, K_P and K_I are the proportional and integral gains of the PI controller, respectively, f_{nom} is the nominal frequency, and H_{filter} is the complex gain of the measurement filter at nominal frequency. References [25],[27] have presented more details about the parameters. The measurement filter is of low-pass type and is intended to remove the high-frequency harmonics of the sampled current and voltage waveforms at the grid-side converter (GSC) and machine-side converter (MSC) terminals. The cut-off frequency depends on the sampling frequency, and example values reported in the literature are in the range of 2 to 5 kHz [25],[27].

As (2) shows, $\bar{Z}_{WTG}$ depends on the parameters of the choke filter, measurement filter and current controller. As shown in Table 1, this impedance takes very large values. A second order Butterworth measurement filter is used to obtain the impedance values in Table 1, and the cut-off frequency is varied in a wide range to give a presentation of possible impedance values.

It should be emphasized that since the equivalent impedance representation assumes steady-state conditions, the impedance values do not vary with time.

B. FSC WTG with a Specific DSC

Per VDE-AR-N 4120, the negative sequence reactive current is proportional to the voltage by a factor defined as the characteristic proportional gain that varies between 2 and 6. Therefore, the equivalent negative sequence impedance varies between 0.167 and 0.5 in pu.

TABLE 1. THE EQUIVALENT NEGATIVE-SEQUENCE IMPEDANCE OF AN FSC WTG WITH CSC.

Measurement filter (2nd order Butterworth)		$\bar{Z}_{WTG}$		
		$R+jX=$ 4.5+j0.45 pu	$R+jX=$ 1.5+j0.15 pu	$R+jX=$ 1.5+j0.15 pu
Cut-off frequency	Phase shift at 60 Hz	$H_g^{PI}=$ 0.387-j0.015 pu	$H_g^{PI}=$ 0.212-j0.015 pu	$H_g^{PI}=$ 0.154-j0.014 pu
100 kHz	-0.05°	1142 pu ∠156°	420 pu ∠144°	384 pu ∠152°
10 kHz	-0.49°	118 pu ∠157°	43 pu ∠144°	40 pu ∠153°
1 kHz	-4.87°	15 pu ∠163°	5 pu ∠152°	5 pu ∠160°

C. DFIG WTG

The DFIG WP model used in this paper is detailed in [26]. This EMT model has been validated using manufacturer specific model [28] and using fault records of two different WPs subjected to different type of unbalanced faults [29]. It is an aggregated model of 1.5-MW DFIG-based WTGs interfaced to the grid through a collector grid and a wind park transformer. The model of each turbine unit consists of mechanical parts, an induction machine, wind turbine transformer, control system, filters, and an ac-dc-ac converter system consisting of a rotor-side converter (RSC) and a GSC. A dc resistive chopper is used for the dc bus over-voltage protection. The WTG is connected to a medium voltage (MV) collector grid through a transformer.

The calculation of the negative-sequence impedance of DFIG WTG is more complex due to machine equations. Per [26], an approximation of its negative-sequence impedance is

$$\left|\bar{Z}_{WTG}\right| \approx \frac{2}{\sqrt{\left|Y_{ds}^{SFR}\right|^2+\left|Y_{qs}^{SFR}\right|^2-2\left|Y_{ds}^{SFR}\right|\left|Y_{qs}^{SFR}\right|\sin\left(\varphi_{Yds}^{SFR}-\varphi_{Yqs}^{SFR}\right)}} \quad (3)$$

$$\angle\varphi_{\bar{Z}_{WTG}} \approx \arctan\left(\frac{\left|Y_{qs}^{SFR}\right|\sin\left(\varphi_{Yqs}^{SFR}\right)+\left|Y_{ds}^{SFR}\right|\cos\left(\varphi_{Yds}^{SFR}\right)}{\left|Y_{ds}^{SFR}\right|\sin\left(\varphi_{Yds}^{SFR}\right)-\left|Y_{qs}^{SFR}\right|\cos\left(\varphi_{Yqs}^{SFR}\right)}\right).$$

The superscripts "SFR" and "SVR" refer to the Stator Flux Reference frame and the Stator Voltage Reference frame, respectively. The subscripts "d" and "q" refer to the *d*- and *q*-axis components of a variable, respectively. The subscript "s" signifies a stator variable. $Y_{ds}^{SFR}=\left|Y_{ds}^{SFR}\right|\angle\varphi_{Yds}^{SFR}$ and $Y_{qs}^{SFR}=\left|Y_{qs}^{SFR}\right|\angle\varphi_{Yqs}^{SFR}$ are complex coefficients which depend on the electrical parameters of the machine, slip and complex gains of the inner controller of the RSC and measurement filter. The negative sequence representation above (see [13] and [26]) is also confirmed in [29] through field measurements.

Table 2 presents the typical values of $\bar{Z}_{WTG}$ for a DFIG WTG which are significantly lower than those of an FSC. t_{rise}^{RSC} signifies the rise-time of the RSC inner loop controller. $Z_{series}=R_s+R_r+j(X_{ls}+X_{lr})$ is the total series impedance of the machine with R_s, R_r, X_{ls}, and X_{lr} being the stator and rotor resistance and leakage reactance at nominal frequency, respectively. X_m denotes the magnetizing reactance at the nominal frequency.

As seen the control parameters have a negligible impact on $\bar{Z}_{WTG}$. The impact of the measurement filter is less considerable than that of t_{rise}^{RSC} which impacts the phase angle of $\bar{Z}_{WTG}$ more than its amplitude. X_m has a negligible impact while $\left|Z_{series}\right|$ has a considerable impact on the amplitude of $\bar{Z}_{WTG}$ which gets larger with increasing $\left|Z_{series}\right|$.

TABLE 2. THE EQUIVALENT NEGATIVE-SEQUENCE IMPEDANCE OF A DFIG WTG AS A FUNCTION OF CONTROL AND MACHINE PARAMETERS.

	$\bar{Z}_{WTG}$		
Control parameters			
Measurement filter phase shift at 60 Hz	t_{rise}^{RSC}		
	10 ms	15 ms	40 ms
-1°	0.34 pu ∠-112.3°	0.33 pu ∠-107.9°	0.32 pu∠ -102.0°
-4°	0.34 pu ∠-113.6°	0.33 pu ∠-109.1°	0.32 pu∠ -103.1°
Machine parameters			
$\left\|Z_{series}\right\|$	X_m = 2 pu	2.9 pu	5 pu
0.2 pu	0.19 pu ∠-108.1°	0.19 pu∠-108.6°	0.20 pu∠-109.4°
0.345 pu	0.33 pu ∠-107.3°	0.33 pu∠-107.9°	0.34 pu∠-108.6°
0.6 pu	0.56 pu ∠-106.2°	0.57 pu∠-106.9°	0.58 pu∠-107.8°

D. Negative-sequence Impedance of Synchronous Generator

An SG does not generate negative sequence current (or voltage). However, its windings provide a low impedance-circulating path to negative sequence current. Hence, an unbalanced grid fault may cause circulation of very large negative sequence current through an SG.

For fault analysis and fault current calculations, an SG is represented by its negative sequence impedance in the negative sequence network of the system. The resistance part of the machine's negative sequence impedance is much smaller than the reactance part. If no further data is available, the negative-sequence impedance of an SG can be approximated by the arithmetic average of the *d*- and *q*-axis sub-transient reactances X_d'' and X_q''. The typical negative-sequence impedance of an SG has an amplitude of approximately 0.12–0.4 pu at a phase angle of -90° where the negative sign is due to the defined current direction [30], [31]. When compared to WTGs:

- Its amplitude is smaller resulting in larger negative-sequence fault currents enabling the operation of 50Q and 51Q elements;
- Its phase angle is different than that of WTGs. The protection element 67Q is set under the assumption of an SG dominated power system. The element uses the phase angle to detect fault direction based on the consideration that a fault in front of the relay causes the negative-sequence voltage measured by the relay to lag the measured negative-sequence current by about 90° whereas a fault behind the relays causes the measured negative-sequence voltage to lead the measured negative-sequence current by about 90°. This assumption is valid in SG dominated power systems where both the source and the grid impedances are highly reactive. Nevertheless, under WTGs, the angular relation may become considerably different particularly for FSC WTG under CSC as shown in Table 1, making the misoperation of the 67Q element more likely.

As the focus of this paper is the impact of IBRs on performances of negative sequence quantities-based protection

elements, only the negative-sequence fault current characteristics of IBRs are analyzed and compared with SGs. Reader should refer to [12], [13], [26] and [28] for the detailed analysis of fault current contributions of IBRs and associated phasor domain models that can be used in short-circuit packages.

III. Protection Malfunction Case Studies

The previous section discussed the potential negative impacts of WTGs on the 50Q, 51Q, and 67Q elements by comparing the negative-sequence impedances of WTGs and SGs. This section provides examples of such malfunctions using Electromagnetic Transient Program (EMTP) simulation case studies on a realistic test system presented in Fig. 2. The system consists of 15 buses marked by (1)-(15) at three voltage levels of {315, 230, 120} kV incorporating 5 WPs marked by WP1-WP5. There are two connection points to the rest of the grid represented by Sys1 (at 315 kV level) and Sys4 (at 120 kV level). Minimum loading condition has been considered, and all loads connected to the 25-kV side of the transformers consume 30 MW at unity power factor. Other system details are presented in Appendix.

Table 3 compares the simulated impedances with the analytical impedances suggesting an acceptable match.

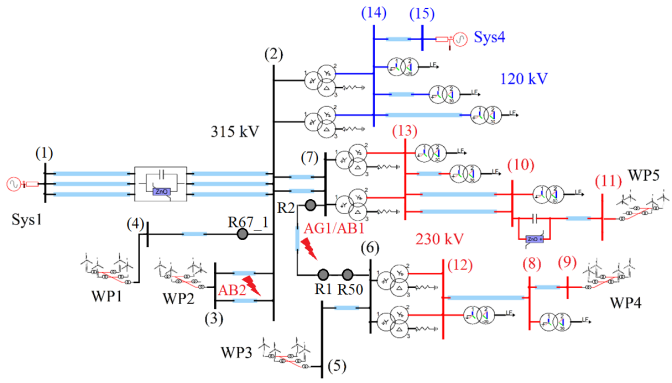

Fig. 2. Test system.

TABLE 3. Simulated versus Analytical Negative-Sequence Impedance of WP3 and WP4.

WTG	$Z_{\bar{W}TG}$	
	Simulation	Analytical*
WP3	4.36 pu ∠19.0°	4.47 pu ∠20.4°
WP4	4.80 pu ∠28.0°	4.47 pu ∠20.4°
*Calculated based on (2) assuming $R+jX=0.005+j0.001$ pu, $H_g^{PI}=0.427-j0.862$ pu, and a 2nd order Butterworth measurement filter with a cut-off frequency of 2.5 kHz. The base of per-unit values are the nominal power and voltage of WTGs.		

A. 50Q Malfunction

The 50Q element operates when the amplitude of the negative-sequence current exceeds a certain threshold and is used to detect unbalanced faults. This element is typically used in transmission line ground fault detection and in conjunction with other protective elements, e.g., in a fault detector scheme supervising directional negative-sequence elements [32], time overcurrent relays, and distance relays which use negative-sequence current for remote backup protection [33].

A permanent phase-A-to-G fault denoted by AG1 is applied at t=1 s. A multifunctional relay containing a 50Q element denoted by R50 on bus 6 protects the faulted line. A stand-alone negative sequence overcurrent relay is rarely applied in transmission phase fault protection applications; this case study is only intended to show the performance of the 50Q element. Table 6 presents the settings of 50Q. The nominal current is set at 1000A which is the amplitude of the positive-sequence current flowing through the transmission line when all WPs are generating rated power. The negative-sequence pick-up current I_{2pkp} has been set at 0.2 pu [34]. The internal protection of WTGs is not considered to give a presentation of the full trajectory of negative-sequence current in all studied cases. Four scenarios have been considered in which the generators of the test system are SG, DFIG, FSC under CSC, and FSC under DSC following the technical connection rules outlined in VDE-AR-N 4120 assuming a proportional gain of 6. Conducted simulations showed that lower values of this gain may not produce enough negative-sequence current to operate the 50Q element of relay R50 for some faults along line (6)-(7). Hence, the gain was set at its maximum recommended value to ensure that the faults are detected.

Fig. 3 shows the apparent amplitude of the negative-sequence fault current measured by relay R50 and the 50Q signal. As shown, the measured negative-sequence fault current is {0.78, 0.52, 0.14, 0.65} pu under SG, DFIG, FSC with CSC, and FSC with DSC, respectively. Under SG, the amplitude of the fault current is greater than the negative-sequence pickup current, and 50Q picks up successfully. The operation is also successful under DFIG. By contrast, for FSC under CSC, the amplitude of 0.14 pu is not large enough to operate the element and hence 50Q fails to assert. With FSC under DSC, this misoperation is resolved as the amplitude of the negative-sequence current increases to 0.65 pu. This increased amplitude is due to the GSC control injecting a negative sequence current with an amplitude proportional to the amplitude of the negative-sequence voltage at the GSC terminal.

Table 4 compares the negative-sequence fault current under DFIG and FSC WTGs assuming coupled and decoupled GSC control options. The results suggest that the amplitude is generally smaller under FSC CSC compared to DFIG making 50Q misoperation more likely under FSC CSC. This is consistent with the finding of Section II that the amplitude of the negative-sequence impedance is larger under FSC CSC.

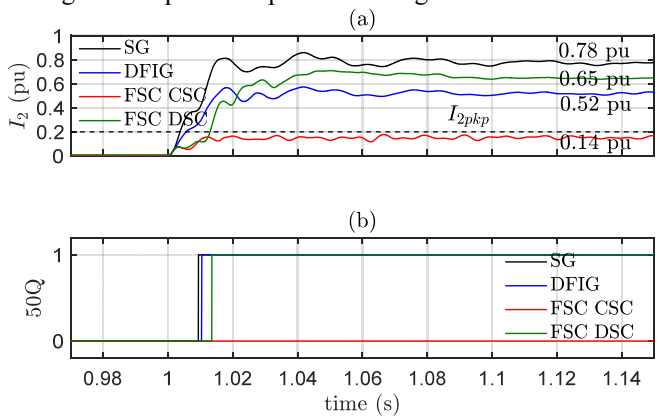

Fig. 3. Relay R50 records under fault AG1: (a) the measured amplitude of the negative-sequence fault current and (b) the 50Q signal under SG (black), DFIG WTG (blue), FSC WTG under CSC (red), and FSC WTG under DSC.

TABLE 4. THE AMPLITUDE OF NEGATIVE-SEQUENCE FAULT CURRENT MEASURED BY R50 DUE TO FAULT AG1.

Generator type	Negative sequence current
SG	0.78 pu
DFIG	0.52 pu
FSC CSC	0.14 pu
FSC DSC	0.65 pu

Recommendations— The main cause of a potential 50Q misoperation is the reduced negative-sequence current level due to WTG controls. A solution to circumvent this problem is to reduce I_{2pkp} setting. However, this solution may not be practical if the required I_{2pkp} setting is too small causing the element to unintentionally respond to unbalanced loading conditions. In protective relaying, relay sensitivities are generally set at a level high enough to tolerate load unbalances under normal operating conditions. Another challenge associated with this solution is the dependency of the negative-sequence fault current on WTG type and control scheme, which makes the finding of an adequate I_{2pkp} setting challenging.

B. 67Q Malfunction

The 67Q element is used in phase fault and ground fault protection [35]. Commonly, the element does not operate alone and is part of a scheme with other elements such as those of overcurrent and distance protection. The element determines the direction of all fault types except the three-phase fault. The operation of the 67Q element relies on the presumption that the generator and grid impedance are predominantly inductive. This assumption may not hold in operating conditions with high shares of power coming from WTGs, potentially causing the misoperation of the 67Q element.

To show this misoperation, a permanent phase-A-to-B fault denoted by AB2 has been applied on the line connecting bus (2) to (3) at t=1 s. A time-overcurrent relay denoted by R67_1 placed at bus 2 looking towards WP1 detects the fault direction. The 67Q element supervises both the phase and the negative-sequence overcurrent elements. Table 6 in the appendix presents the settings of R67_1. The rated current is set at 550A. The forward and reverse direction pickup currents $I_{pkpForward}$ and $I_{pkpReverse}$ are set at 0.25 pu and 0.15 pu, respectively, and the Maximum Torque Angle (MTA) is set at 85° based on the line angle of the protected power line. Similar to the previous case, the study considers four cases where generators are SG, DFIG, FSC under CSC, or FSC under DSC assuming the same rating and output power. Successful operation means 67Q_1 sees fault AB2 as reverse.

Fig. 4 shows the oscillographic data and the response of R67_1. The phase angle has been measured at 100 ms into the fault, I_2 and V_2 stand for the apparent amplitude of the negative-sequence current and voltage, and 67Q2 and 67Q3 represent the forward and reverse direction signals, respectively. As Fig. 4(a) shows, under SG the relay sees a phase angle difference of approximately 87.4° with V_2 leading I_2, the equivalent negative-sequence impedance vector falls within the reverse zone of the impedance plane, and the relay successfully issues 67Q3 declaring reverse direction. The operation is also successful under DFIG (Fig. 4 (b)) where the apparent V_2 leads I_2 by about 78°. Nevertheless, under FSC CSC neither 67Q2 nor 67Q3 pick up, and the relay fails to detect the direction. The reason is that the negative-sequence current amplitude is smaller than the pickup current setting of 0.2 pu, and hence, 67Q does not pick up. To study whether this misoperation can be fixed by reducing the pickup setting, $I_{pkpForward}$ and $I_{pkpReverse}$ have been reduced to 0.02 pu; this setting is too small compared to typical and is not used in practice; however, it is used in this case study to investigate the angular relation of negative-sequence quantities under FSC. Fig. 4 (d) shows the results suggesting that the reduced pickup threshold causes R67_1 to pick up; however, the element mistakenly declares forward direction and issues 67Q2. The reason is that the apparent phase angle difference becomes about -20° (I_2 leading V_2), and hence the equivalent negative-sequence impedance falls within the forward detection zone. The results are consistent with the analysis of Section II that the misoperation of 67Q is more likely under FSC CSC compared to DFIG. Fig. 4 (e) shows that the adoption of DSC based on VDE-AR-N 4120 resolves the misoperation since the apparent phase angle becomes 91.5° which is within the reverse zone.

Discussion— The apparent phase angle difference between negative-sequence current and voltage is determined by the impedance between the source and the fault point and hence is a function of line angle. The German grid code VDE-AR-N 4120 does not consider line angle and only requires the WTG to inject a negative-sequence reactive current. If line angle is not close to 90°, it may not be possible under the WTG DSC to maintain the same angular relation between negative-sequence current and voltage as that under a SG on buses away from the generator bus. The reason is the limited amplitude of the injected I_2 due to WTG converter current limits. In such a case, the angle measured by the 67Q element may be different under WTG DSC compared to SG. This difference did not cause a 67Q misoperation in conducted simulations on the test case of Fig. 2 since the angle difference was within the angle margin the 67Q element (forward and reverse limit angles of ±80°). In case the injected I_2 of the WTG is not sufficiently large, the line angle is significantly different than 90°, and the margin of the 67Q element is insufficient, then the German grid code may not resolve the 67Q misoperation, and other solutions should be considered.

1) Impact of WTG Type

Table 5 shows the apparent phase-angle under different WTG types (DFIG or FSC) suggesting that the phase angle, and hence the performance of 67Q, is significantly dependent on the type. The results further suggest that 67Q misoperation is more likely with FSC, which is consistent with the finding of Section II. In the studied scenarios, the misoperation did not occur with DFIG; however, field measurements imply that misoperation might also occur under DFIG [21].

2) Impact of GSC Control

Table 5 further compares the measured phase angle under CSC and DSC. Conducted simulations suggest that the impact of GSC control is more considerable under FSC compared to DFIG. This is expected because in DFIG, the machine predominantly determines the negative-sequence behavior, and the converter has a negligible contribution. The results further suggest that 67Q misoperation is more likely under CSC

compared to DSC. In the studied cases, the adoption of VDE-AR-N 4120 resolved the misoperation. The reason is that the code requires the injected negative sequence current to lead negative sequence voltage by 90° thereby emulating the behavior of an SG and satisfying the condition required for correct operation of the 67Q element.

Recommendations— The general recommendation of this case study is that 67Q cannot be applied when a resource is unable to supply enough negative sequence inductive current.

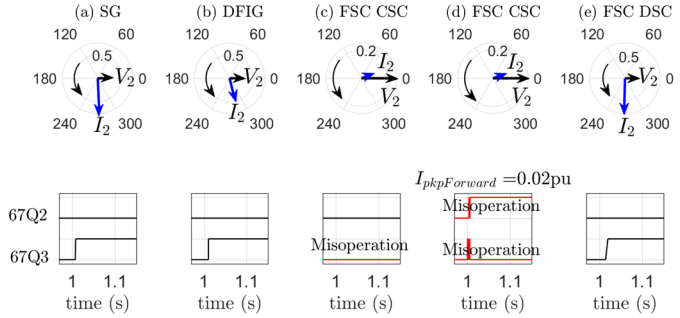

Fig. 4. Relay R67_1 records in response to fault AB2 under SG, DFIG WTG, FSC WTG under CSC, and FSC WTG under DSC.

TABLE 5. THE PHASE-ANGLE OF THE NEGATIVE-SEQUENCE IMPEDANCE MEASURED BY R67_1 DUE TO FAULT AB2.

Generator type	Phase Angle of the Negative Sequence Impedance
SG	87.4°
DFIG	78.0°
FSC CSC	-20.0°
FSC DSC	91.5°

IV. IMPACTED PROTECTION FUNCTIONS

Section III has illustrated the misoperation of the 51Q and 67Q elements due to WTGs. As mentioned in the introduction, these elements are seldom used alone and are commonly part of a larger protection scheme. Hence, the misoperation of these elements may cause the misoperation of other protection schemes.

A. Communication-Assisted Protection

The objective of communication-assisted protection is to provide high-speed tripping from both ends of a protected line for faults along the entire line segment [36], [37]. The most prevalent communication-assisted protection schemes include Permissive Overreaching Transfer Trip (POTT), Permissive Underreaching Transfer Trip (PUTT), Directional Comparison Blocking (DCB), and Directional Comparison Unblocking (DCUB). All schemes use distance and directional elements to determine the status of each line terminal. Distance Zone 2 (forward) and Zone 3 (reverse) are used by all schemes while Zone 1 and Zone 4 are optional. Directional elements including level 2 and 3 elements, such as 67Q2 and 67Q3, are also used to provide more sensitive fault detection for unbalanced faults and can either supplement or replace ground distance (zone) elements in communications-assisted trip schemes.

The use of 67Q renders the communication-assisted tripping prone to malfunction under WTGs. Basically, the possible failure of the directional element causes the scheme not to key the permissive trip to the remote relay. It should be mentioned that the use of negative-sequence directional supervision in pilot protection is for additional security benefit but is not essential.

To show a misoperation example, a POTT scheme has been added to the test system of Fig. 2 to protect the line connecting buses (6) and (7), and fault AG1 has been repeated. The POTT scheme uses overreaching zone 2 elements supervised by an additional directional negative-sequence element [38]. A trip requires the overreaching zone 2 elements to be picked up and permission to be received from the remote end. Two multi-function relays denoted by R1 and R2 realize the POTT scheme based on 21G_Z2 (ground distance zone 2) and 67Q. The POTT scheme should clear fault AG1 instantaneously. Successful POTT operation requires both 21G_Z2 and 67Q2 to be picked up by R1 and R2 to key the permissive trip to the respective remote relay, and 21G_Z2 of each relay to trip on receipt of the permissive trip. Three generation scenarios have been considered: first where WP1-WP5 are SGs, second where they are FSC WTG with CSC, and third where they are FSC WTG with DSC.

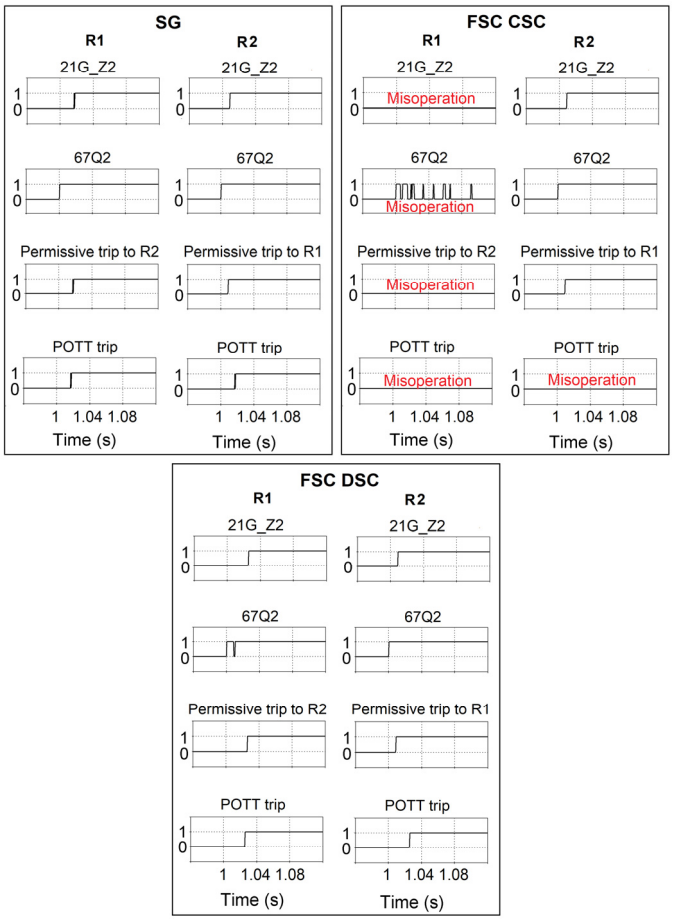

Fig. 5. POTT misoperation case study: Response of relays R1 and R2 to fault AB1 under SG, and FSC WTG with CSC, and FSC WTG with DSC.

Fig. 5 shows the simulation results. Under SG, R1 sees the fault in zone 2 and forward direction, issues both 21G_Z2 and 67Q2, and keys permission to trip to R2. Similarly, R2 sees the fault in zone 2 and forward direction, issues both 21G_Z2 and 67Q2, and keys permissive trip to R1. Both R1 and R2 receive permission from their respective remote end, and POTT operates successfully. Under FSC WTG with CSC, 67Q2 of R1 asserts only transiently hence, R1 fails to key permission to R2, and POTT malfunctions. The malfunctioning element is 67Q2

of R1, and the cause of misoperation is the negative-sequence impedance phase angle of about -180°, which does not fall within the forward or reverse zone of R1. Because of this misoperation, the POTT scheme of the remote relay fails to trip for the in-zone AG1 fault. This misoperation is fixed under DSC control mode. In this case, due to the negative-sequence reactive fault current contribution of WP3 and WP4, the 67Q element of R1 successfully issues 67Q2, permissive trip is keyed to R2, and POTT operates successfully.

This case study illustrates that DSC control is a potential solution to the potential misoperation of communication-assisted protection under FSC WTG. Reference [21] has presented another solution using POTT scheme with zero-sequence and echo logic to provide ground fault protection of transmission interconnection of IBRs. The case study of this paper does not include echo logic.

B. Fault Identification

FID is used by protective elements to identify the type of a fault and the faulted phase(s) for applications such as signal processing economy where a relay selects different algorithm elements to deal with different fault situations [39],[40], improved accuracy of distance relaying schemes [41], and restraining ground distance elements during double-line-to-ground faults [38],[40]. In one implementation of the FID logic the phase angle relationship between the negative- and zero-sequence current IA2 and IA0 is used to identify the faulted phase loop. This angle is compared to a plurality of successive angle ranging from 0 to 360° defined by corresponding sectors. The operation principle is as follows [42]. If the phase angle between IA2 and IA0 is 0°±{a phase margin} (the yellow sector in Fig. 6), the fault type is either AG or BCG, and the relay enables AG and BC elements only. In this sector, the relay selects AG or BCG based on which element has the lowest calculated reach. If IA2 lags IA0 by 120°±{a phase margin} (the red sector in Fig. 6), the fault type is either BG or CAG, and the relay enables BG and CA elements only. In this sector, the relay selects BG or CAG based on which element has the lowest calculated reach. Finally, if IA2 leads IA0 by 120°{±a phase margin} (the green sector in Fig. 6), the fault type is either CG or ABG, and the relay enables CG and AB elements only. In this sector, the relay selects CG or ABG based on which element has the lowest calculated reach. The margin angle is a setting of FID used to ensure proper phase selection under varying fault resistances [42].

The impact of WTGs on the phase angle of the negative sequence current IA2 may negatively influence the operation of FID. IA2 may not fall within the defined sectors for a given fault type under WTGs and cause an incorrect phase selection by FID. To illustrate such a misoperation, fault AG1 has been repeated. Relay R1 incorporates an FID based on the above-mentioned detection logic with a phase margin of 30°. Fig. 6 shows IA2 and IA0 phasors superimposed on the phase selection sectors and the response of the FID of R1 to an AG fault under SG, FSC WTG with CSC, and FSC WTG with DSC. Under SG, IA2 lags IA0 by about 6° which falls within the AG sector of the FID, and R1 declares phase A as the faulted phase by issuing the FID_A signal. However, under FSC WTG with CSC, IA2 leads IA0 by 80° which does not fall within any FID sector and hence, FID fails to detect the faulted phase. Under FSC WTG DSC, the FID correctly detects the faulted phase.

It should be mentioned that FID using negative and zero sequence current is only initiated if the zero and negative-sequence currents are above a certain threshold (relay setting). If this is not the case, FID is done using voltages [38]. In the studied case, the current-based FID operated in all considered scenarios and voltage-based FID did not operate.

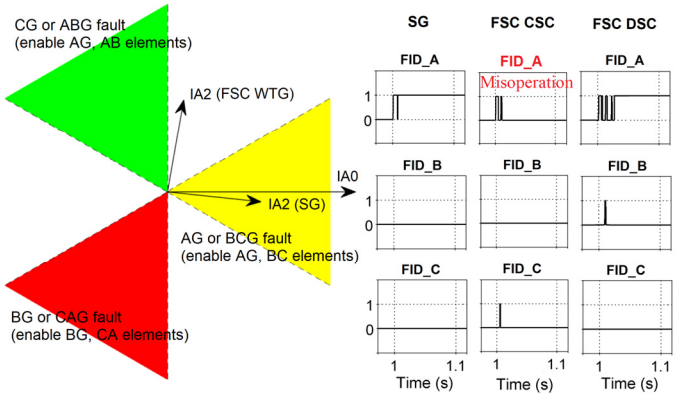

Fig. 6. FID misoperation case study: IA2 and IA0 phasors superimposed on the phase selection sectors and the response of the FID of R1 to the AG fault under SG, FSC WTG with CSC, and FSC WTG with DSC.

V. Experimental Validation

To further illustrate the misoperation of negative sequence quantities-based protection elements due to wind generation, an experimental test has been carried out using an HIL setup shown in Fig. 7. The relay under test is a distance relay which uses a negative sequence overcurrent element. The experiment studies the performance of this element under wind generation.

In addition to the distance relay, the simulation loop consists of a digital simulator, a voltage and current amplifier, and a computer realizing a Simulink simulation model of a transmission system including a complete WTG model translated from EMTP. To subject the relay to a given fault, first the fault is simulated in the simulation model running on the digital simulator. The simulator calculates the instantaneous voltage and current waveforms at the assumed location of the relay in the simulation model and supplies them to the amplifier through analog output ports as low-power voltage signals. The amplifier transforms these low-power voltage signals into high-power 110 V and 1 A voltage and current waveforms which are then supplied to the current and voltage input terminals of the relay. Finally, the relay operates on these voltage and current inputs and sends the trip signal back to the simulation model through an analog input port.

The studied fault is a mid-line (50% of the line length) 100-ms phase-A-to-ground fault on a transmission line connecting an FSC WTG with CSC to the rest of the transmission system. The distance relay is assumed to be located at the WTG bus looking towards the faulted line; the activated protection functions of the relay include distance element zone 1 whose reach is set at 80% of the line length and the directional negative-sequence element. Successful relay operation means

that the relay sees the fault as Zone 1 forward. Two scenarios have been considered comparing relay performance under SG and FSC WTG with CSC. Under SG, the directional element declared the fault as forward. However, under FSC the directional element mistakenly classified the fault as reverse. This misoperation further verifies the conclusion of this paper that wind generation may adversely impact the performance of the directional element because of the changed phase angle relation of negative-sequence voltage and current.

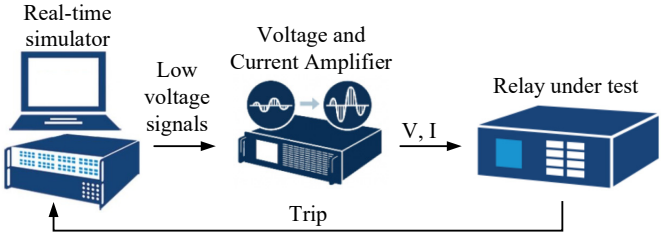

Fig. 7. Experimental setup for testing the performance of a distance relay under wind generation.

VI. Conclusion

WPs may negatively affect the performance of protection schemes based on negative sequence components. The paper has identified two main causes for such a misoperation: (i) the smaller negative-sequence fault current contribution of a WTG compared to an SG and (ii) the changed angular relation of negative-sequence current and voltage phasors under WPs. The former may cause the misoperation of negative-sequence overcurrent elements (50Q/51Q) and the latter may result in the misoperation of directional negative-sequence overcurrent element (67Q). The paper has provided examples of such a misoperation using simulation case studies. Here are the main findings of the paper:

- WTG type (DFIG or FSC) and GSC control (CSC or DSC) are key factors influencing the performance of 50Q/51Q and 67Q elements.
- Regarding WTG type, 50Q and 67Q are more likely to malfunction under FSC compared to DFIG due to lower negative-sequence fault current contribution of FSC. This conclusion holds under CSC.
- Concerning GSC control mode, 50Q is more likely to malfunction under CSC due to the suppression of negative-sequence current. 67Q is also more likely to malfunction under CSC control due to the changed phase angle of the negative-sequence current and voltage phasors. A potential solution to 50Q misoperation is to pick an adequate DSC. Potential solutions to 67Q misoperation include picking an adequate DSC or changing the setting of the 67Q element.
- The number of WTG units in service could affect both the amplitude and phase angle of the negative-sequence fault current and hence the performance of both 50Q/51Q and 67Q. This paper left out these scenarios due to space constraints.

As shown in this paper, malfunctioning of the 67Q element may result in misoperation of communication-assisted protection. When 67Q element does not function, the relay fails to send a permissive trip key to the remote relay, and the POTT scheme fails to trip for an in-zone fault. In addition, the FID may not work properly due to a shift in the phase angle of the negative-sequence current as shown in this paper.

VII. Appendix: Parameters of the Test System

Table 6 presents the parameters of the test system of Fig. 2.

Table 6. Parameters of the Test System of Fig. 2.

WP parameters					
WP	Type	Installed capacity	# of units in service	Wind speed	Active power at the POI
WP1	III	200 x 1.5 MW	100	0.6 pu	32.6 MW
WP2	IV	150 x 1.5 MW	150	1.0 pu	219.8 MW
WP3	IV	200 x 1.5 MW	200	1.0 pu	293.0 MW
WP4	IV	133 x 1.5 MW	133	1.0 pu	194.9 MW
WP5	III	200 x 1.5 MW	200	0.6 pu	65.2 MW

Settings of relay R50	
Setting	Value
Nominal current	1000 A (1 pu)
Negative-sequence pickup current I_{2pkp}	0.2 pu

Settings of relay R67 1	
Rated current	550 A (1 pu)
MTA	85°
Forward limit angle	80°
Reverse limit angle	80°
$I_{pkpForward}$	0.25 pu
$I_{pkpReverse}$	0.15 pu

References

[1] "Impact of inverter-based generation on bulk power system dynamics and short-circuit performance", PES-TR68, prepared by the IEEE/NERC Task Force on Short-Circuit and System Performance Impact of Inverter Based Generation, Jul. 2018.

[2] WSPPID/WSPI/WSPI-P - Wind and Solar Plant Interconnection Performance Working Group (WSPI-P), "P2800─Standard for interconnection and interoperability of inverter-based resources interconnecting with associated transmission electric power systems," PAR approval, Sep. 2018.

[3] J. Martinez, P. C. Kjar, P. Rodriguez, and R. Teodorescu, "Short circuit signatures from different wind turbine generator types," in *Proc. 2011 IEEE Power Systems Conference and Exposition*, Phoenix, AZ, Mar. 20-23, 2011.

[4] IEEE PES Joint Working Group, "Fault current contributions from wind plants," Technical Report, Oct. 2013.

[5] E. Farantatos, U. Karaagac, H. Saad, and J. Mahseredjian, "Short-circuit current contribution of converter interfaced wind turbines and the impact on system protection," *Bulk Power Systems Dynamics and Control – IX (IREP)*, Rethymnon, Crete, Greece, Aug. 25–30, 2013.

[6] M. Fischer and A. Mendonca, "Representation of variable speed full conversion wind energy converters for steady-state short circuit calculations," in *Proc. IEEE PES Transmission & Distribution Conference & Exposition*, Orlando, FL, May 7–10, 2012.

[7] D. F. Howard, "Short circuit currents in wind-turbine generator networks," Ph.D. Thesis, Georgia Institute of Technology, Dec. 2013.

[8] D. F. Howard, J. Liang and R. G. Harley, "Short-circuit modeling of DFIGs with uninterrupted control," *IEEE J. Emerging and Selected Topics in Power Electron.*, vol. 2, no. 1, pp. 47–57, Mar. 2014.

[9] U. Karaagac, T. Kauffmann, I. Kocar, H. Gras, J. Mahseredjian, B. Cetindag, and E. Farantatos, "Phasor domain modeling of type-IV wind turbine generator for protection studies," *IEEE Power Energy Soc. Gen. Meeting*, 2015.

[10] I. Kocar, T. Kauffmann, U. Karaagac, J. Mahseredjian, and E. Farantatos, "Phasor domain modeling of full scale frequency converters for protection studies," 4th International Workshop on Integration of Solar Power into Power Systems, Berlin, Germany, Nov. 2014.

[11] T. Kauffmann, U. Karaagac, I. Kocar, H. Gras, J. Mahseredjian, B. Cetindag, and E. Farantatos, "Phasor domain modeling of type-III wind turbine generator for protection studies," *IEEE Power Energy Soc. Gen. Meeting*, 2015.

[12] T. Kauffmann, U. Karaagac, I. Kocar, S. Jensen, E. Farantatos, A. Haddadi and J. Mahseredjian, "Short-Circuit Model for Type IV Wind

Turbine Generators with Decoupled Sequence Control," *IEEE Trans. Power Del*., vol. 34, no. 5, pp. 1998-2007, Oct. 2019.
[13] T. Kauffmann, U. Karaagac, I. Kocar, S. Jensen, J. Mahseredjian, and E. Farantatos, "An accurate type III wind turbine generator short circuit model for protection applications," *IEEE Trans. Power Del*., vol. 32, no. 6, pp. 2370–2379, Dec. 2017.
[14] A. Hooshyar, M. A. Azzouz, and E. F. El-Saadany, "Distance protection of lines connected to induction generator-based windfarms during balance faults," *IEEE Trans. Sustain. Energy*, vol. 5, no. 4, pp. 1193–1203, Oct. 2014.
[15] A. Hooshyar, M. A. Azzouz, and E. F. El-Saadany, "Distance protection of lines emanating from full-scale converter-interfaced renewable energy power plants–Part I: Problem statement," *IEEE Trans. Power Del*., vol. 30, no. 4, pp. 1770–1780, Aug. 2015.
[16] A. Hooshyar, M. A. Azzouz, and E. F. El-Saadany, "Distance protection of lines emanating from full-scale converter-interfaced renewable energy power plants – Part II: Solution description and evaluation," *IEEE Trans. Power Del*., vol. 30, no. 4, pp. 1781–1791, Aug. 2015.
[17] L. He, C. C. Liu, A. Pitto, and D. Cirio, "Distance protection of AC grid with HVDC-connected offshore wind generators," *IEEE Trans. Power Del*., vol. 29, no. 2, pp. 493–501, Apr. 2014.
[18] S. Srivastava, A. Biswal, S. Ganesan, and U. J. Shenoy, "Behavior of self-polarized Mho characteristic on lines fed from DFIG based wind farms," *IEEE Innovative Smart Grid Tech.-Asia*, Bangalore, Nov. 10–13, 2013.
[19] A. Haddadi, I. Kocar, U. Karaagac, H. Gras, and E. Farantatos, "Impact of wind generation on power swing protection," *IEEE Trans. Power Del.*, vol. 34, no. 3, pp. 1118–1128, Jun. 2019.
[20] G. Kou, L. Chen, P. VanSant, F. Velez-Cedeno and Y. Liu, "Fault characteristics of distributed solar generation," *IEEE Trans. Power Del.* (Early access), Mar. 2019.
[21] M. Nagpal and C. Henville, "Impact of power-electronic sources on transmission line ground fault protection," *IEEE Trans. Power Del*., vol. 33, no. 1, pp. 62–70, Feb. 2018.
[22] I. Erlich, T. Neumann, F. Shewarega, P. Schegner, and J. Meyer, "Wind turbine negative sequence current control and its effect on power system protection," *IEEE Power Energy Soc. Gen. Meeting*, Jul. 2013.
[23] Impact of Renewables on System Protection: Wind/PV Short-Circuit Phasor Model Library and Guidelines for System Protection Studies. EPRI, Palo Alto, CA: 2016, 3002008367.
[24] Technische Regeln für den Anschluss von Kundenanlagen an das Hochspannungsnetz und deren Betrieb (TAR Hochspannung), VDE-ARN 4120 Anwendungsregel: 2018-11.
[25] U. Karaagac et al., "A generic EMT-type model for wind parks with permanent magnet synchronous generator full size converter wind turbines," *IEEE Power and Energy Technology Systems Journal*, vol. 6, no. 3, pp. 131–141, Sep. 2019.
[26] T. Kauffmann, "Modeling of wind parks for steady state short circuit studies," Ph.D. dissertation, Elect. Eng. Dept., École Polytechnique de Montréal, Montréal, Canada, 2018.
[27] U. Karaagac, J. Mahseredjian, S. Jensen, R. Gagnon, M. Fecteau, and I. Kocar, "Safe operation of DFIG-based wind parks in series-compensated systems," *IEEE Trans. Power Del*., vol. 33, no. 2, pp. 709–718, Apr. 2018.
[28] Impact of Renewables on System Protection: Wind/PV Short-Circuit Phasor Model Library and Guidelines for System Protection Studies, Palo Alto, CA: 2016. 3002008367.
[29] A. Haddadi, I. Kocar, T. Kauffmann, U. Karaagac, E. Farantatos and J. Mahseredjian, "Field Validation of Generic Wind Park Models using Fault Records," *J. Mod. Power Syst. Clean Energy*, vol. 7, no. 4, pp. 826–836, Jul. 2019.
[30] J. L. Blackburn, *Symmetrical Components for Power Systems Engineering*, CRC Press, 1993.
[31] P. Kundur, *Power System Stability and Control*, McGraw-Hill, 1994.
[32] F. Calero, "Rebirth of negative-sequence quantities in protective relaying with microprocessor-based relays," Schweitzer Eng. Labs. Inc., 2003.
[33] Y. Ohura, T. Matsuda, M. Suzuki, F. Andow, Y. Kurosawa, and A. Takeuchi, "A digital distance relay using negative sequence current," *IEEE Trans. Power Del*., vol. 5, pp. 79–84, Jan. 1990.
[34] PSRC Working Group D24, "Transmission line applications of directional ground overcurrent relays," IEEE Power System Relaying and Control Committee (PSRC), Jan. 2014.
[35] J. Horak, "Directional overcurrent relaying (67) concepts", in proc. *59th IEEE Conf. Protective Relay Eng*., 2006.
[36] IEEE std. C37.113-2015, "IEEE guide for protective relay applications to transmission lines," Dec. 2015.
[37] R. Patterson, E. Price and M.P. Sanders, "Directional comparison blocking system fundamentals," *the 66th Protective Relaying Conference*, Atlanta, GA, U.S., 2012.
[38] D60 Line Distance Protection System, UR Series Instruction Manual, GE Digital Energy, D60 Revision 7.1x.
[39] G. Ziegler. *Numerical Distance Protection: Principles and Applications*, 4th Edition. Germany: Siemens-Erlangen Publicis, 1999.
[40] E. O. Schweitzer, III, "New developments in distance relay polarization and fault-type selection," in *Proc. 16th Annu. Western Protective Relay Conference*, Spokane, WA, Oct. 1991.
[41] D. W. P. Thomas, M. S. Jones, and C. Christopoulos, "Phase selection based on superimposed components," *Proc. Inst. Elect. Eng.—Gener., Transm. Distrib.*, vol. 143, pp. 295–299, May 1996.
[42] D. Costello and K. Zimmerman, "Determining the faulted phase," *the 63rd Annu. Conf. Protect. Relay Eng.*, College Station, TX, U.S., Mar. 2010.

Aboutaleb Haddadi (St'11–M'15) received the Ph.D. degree in electrical and computer engineering from McGill University, Montréal Canada, in 2015. From 2015 to 2018, he was a Postdoctoral Fellow with Polytechnique Montréal where he is currently a Research Associate. He has consulting experience in the areas of power system transient analysis and simulation and has contributed to the development of various industry-standard power system simulation software. His main research interests include simulation, modeling, and control of power electronic converters, with applications in power systems and power system protection.

Mingxuan Zhao is a full-time electrical engineering PhD student at Polytechnique Montreal. He received his Bachelor's degree in electrical engineering from the Hong Kong Polytechnic University in 2018. He is now researching on resolving protection problems in inverter-based resources dominant future networks.

Ilhan Kocar (SM'13) is a full professor at Polytechnique Montreal in the department of electrical engineering. He received the Ph.D. degree from Polytechnique and University of Montreal in 2009.
He worked as a power electronics engineer at Aselsan Electronics Inc. (1998-2004). He worked as a Software R&D Engineer at CYME International T&D (2009-2011), now part of Eaton Corporation. He joined the faculty at Polytechnique Montreal in 2011.
Ilhan's career highlights include breakthrough contributions to professional simulation tools, and development of solutions for large-scale integration of inverter-based resources. He has performed many grid-consulting projects that cover design, modeling, analysis and validation of field measurements. His research is on the development of concepts, models and methods for the simulation of power systems and large-scale integration of power electronics-based systems into grids.

Ulas Karaagac (M'08) received the Ph.D. degree in electrical engineering from Polytechnique Montreal (affiliated with Université de Montreal), Montreal, QC, Canada, in 2011. From 1999 to 2007, he was an R&D Engineer with the Information Technology and Electronics Research Institute, Ankara, Turkey. He was a Ph.D. Scholar at Polytechnique Montreal between 2007 and 2011, where he continued working as a

Postdoctoral Fellow and then as a Research Associate until the end of 2016. In December 2016, he joined the Department of Electrical Engineering, Hong Kong Polytechnic University, as a Research Assistant Professor. His research interests include integration of large-scale renewables into power grids, HVDC transmission, modeling and simulation of large-scale power systems, and power system dynamics and control.

Ka Wing Chan (M'98) received the B.Sc. (Hons) and Ph.D. degrees in electronic and electrical engineering from the University of Bath, U.K., in 1988 and 1992, respectively. He currently is an Associate Professor and Associate Head in the Department of Electrical Engineering of the Hong Kong Polytechnic University. His general research interests include power system stability, analysis and control, power grid integration, security, resilience and optimization, demand response management, etc.

Evangelos Farantatos (St. M'06, M'13, SM'18) received the Diploma in Electrical and Computer Engineering from the National Technical University of Athens, Greece, in 2006 and the M.S. and Ph.D. degrees from the Georgia Institute of Technology, Atlanta, GA, USA, in 2009 and 2012, respectively. He is a Senior Project Manager with the Grid Operations and Planning R&D Group at EPRI, Palo Alto, CA. He is managing and leading the technical work of various R&D projects related to synchrophasor technology, power systems monitoring and control, power systems stability and dynamics, renewable energy resources modeling, grid operation with high levels of inverter-based resources and system protection. He is a Senior Member of IEEE. In summer 2009, he was an intern at MISO.